Surface Science 636 (2015) 36–41

Contents lists available at ScienceDirect

Surface Science

journal homepage: www.elsevier.com/locate/susc

Cu- and CuO-decorated graphene as a nanosensor for H_2S detection at room temperature

E. Mohammadi-Manesh [a,*], M. Vaezzadeh [a], M. Saeidi [b]

[a] Faculty of Physics, K.N. Toosi University of Technology, Tehran, Iran
[b] Department of Physics, Faculty of Basic Sciences, Shahed University, Tehran, Iran

ARTICLE INFO

Article history:
Received 2 November 2014
Accepted 4 February 2015
Available online 11 February 2015

Keywords:
Graphene
Electrical conductance
Hydrogen sulfide
Copper oxide
Nanosensor
Density Functional Theory (DFT)

ABSTRACT

In this paper, the adsorption mechanism, density of states, charge population analysis and electrical conductance at room temperature are investigated for the detection of hydrogen sulfide (H_2S) gas by pure, and Cu- and CuO-decorated graphene sheets (GS). All calculations are done using density functional theory. Results demonstrate that a CuO-GS structure has higher binding energy with H_2S than Cu-GS, and GS. Moreover, the investigated density of states show that orbital hybridization is obviously different between the H_2S and Cu-GS, and the H_2S and CuO-GS, while there is no evidence for hybridization between the H_2S gas and the GS. Furthermore, to find the best nanosensor, electrical conductance of all the possible configurations before and after H_2S adsorption at room temperature is computationally investigated. The obtained results illustrate that electrical conductance of the CuO-GS is significantly changed by H_2S gas adsorption. So, in normal conditions and at room temperature, the CuO-GS system has more favorable features in the detection of H_2S than the GS, and Cu-GS structures.

1. Introduction

Fast and exact detection of trace amounts of dangerous gases such as hydrogen sulfide (H_2S) is important in many aspects of human society, i.e. in industrial processes, public health, national security and environmental monitoring. Breathing H_2S is reported to be harmful to human health and can be deadly, depending on the exposure condensation and duration; exposure to only 300 ppm for 30 min is enough to render a worker comatose [1]. It also has damaging effects on many industrial catalysts and is known to be a major source of acid rain when oxidized in the atmosphere. Many industrial processes generate considerable quantities of hydrogen sulfide, including natural gas processing, biogas fermentation, coal gasification, petroleum refining, kraft mills, and coke ovens. In recent years, interactions of H_2S with semiconductor and metallic surfaces have been investigated computationally and experimentally due to the promising applications of these systems in nanosensor devices [2–15]. The graphene sheet (GS) is considered as an applicable material in the production of nanosensors [16, 17]. Some experimental researches have shown that the electrical properties of GS can be tuned by doping, and decorating with other atoms, which provide a new route for the preparation of good performance graphene based sensing materials. GS has been successfully decorated with numerous atoms and molecule materials including Ag, Au, Cu, CuO, ZnO, Cu_2O salts by different methods [18–25]. Cu and CuO have attracted a great deal of attention because of their various applications. They have been widely used in many important fields such as gas sensors, solar cells, magnetic phase transitions, superconductors and photocatalysts [26–32]. Production methods of Cu- and CuO-decorated GS (Cu-GS, and CuO-GS) include heating an aqueous solution of Cu salts in the presence of graphene synthesized by an arc discharge method, solvothermal synthesis of CuO-GS and the subsequent reduction of graphene oxide by hydrazine vapor, and chemical reduction of Cu salts in an aqueous solution in the presence of hydrogen induced exfoliated graphene [33–37].

According to the ability of Cu-GS, and CuO-GS production and importance of H_2S detection, a comprehensive theoretical study is needed to investigate H_2S gas adsorption on GS and modified graphene with Cu, and CuO. For the computational investigation of electronic structure, adsorption energy, electrical and thermal conductance variations, etc., one can study the effect of only one atom or molecule adsorption on a specific structure. Reported simulation results by this method are in good agreement with results of experimental studies on nano structures [21, 38]. In addition, this method reduces the time of calculations. However, the results of this approach can be expanded for structures decorated with more atoms or molecules.

In this paper, the adsorption of H_2S on GS, Cu-GS, and CuO-GS configurations is computationally investigated. The excellent adsorption

* Corresponding author.
E-mail address: emanesh@mail.kntu.ac.ir (E. Mohammadi-Manesh).

http://dx.doi.org/10.1016/j.susc.2015.02.002
0039-6028/

geometries, the changes in adsorption energies, and electronic properties during adsorption are studied by using density functional theory (DFT). Also, The electrical conductance of the most stable GS, Cu-GS and CuO-GS systems is calculated at room temperature before and after the adsorption of H_2S gas to find the best nanosensor.

2. Simulation and calculation

Structure, density of state (DOS), partial density of states (PDOS), the Mulliken population analysis, and adsorption energies of the systems are simulated and calculated by QUANTUM ESPRESSO package [39]. This package works based on DFT and using the expansion of plane wave. After the relaxation and investigation of different approximations, generalized gradient approximation (GGA) is chosen with Perdew–Burke–Ernzerhof (PBE) functional type in which density gradient is used in addition to local density approximation to describe exchange-correlation potential. In our calculation, Rappe Rabe Kaxiras Joannopoulos (RRKJUS) method in ultrasoft pseudopotential is used to describe the interaction between electron and ion in carbon, oxygen, copper and hydrogen atoms. Supercell used in the calculations is a GS with 50 carbon atoms. This number of carbon atoms is used to eliminate interaction between adsorbed atoms on a supercell and adsorbed atoms on the neighbor supercell. The distance between layers is optimized to 20 Å considering the minimization of interaction between layers for both before and after adsorption of molecules. The structure of supercell is considered as mentioned form to guarantee the uniformity of expanded supercell structure in space. The kinetic energy cutoff is optimized to 45 Ry. The Monkhorst–Pack method is used for k-points. Number of k-points for relaxation and self-consistent field (SCF) calculations is optimized to $6 \times 6 \times 1$ and for nonself-consistent field (NSCF) calculations is optimized to $8 \times \times 1$ which leads to maximum convergence in energy. Then adsorption energy, DOS, PDOS, charge transfer and orbital hybridization for different configurations of the system are calculated by optimized parameters. In all calculations, the convergence threshold on total energy (a.u) and forces (a.u) are 10^{-8}, and 10^{-7} for ionic minimization, respectively. Also, convergence threshold (conv-thr) for selfconsistency (estimated energy error < conv − thr) is 10^{-10}.

The semiclassical Boltzmann transportation equation is used for the calculation of electrical conductance of different configurations at room temperature by Boltzmann Transport Properties (BoltzTrap) code [40]. The input file for this program is a set of results of the NSCF calculations with a mesh of $30 \times 30 \times 5$ k-points by QUANTUM ESPRESSO. Finally components of conductance tensor are obtained.

All possible orientations for nearing H_2S, Cu, and CuO to GS are shown in Fig. 1. First, the adsorption of a Cu atom, and CuO molecule on the GS is considered. Next, the interaction between H_2S and the GS, Cu-GS, and CuO-GS is investigated. Then, the electrical conductance at room temperature for three structures before and after H_2S adsorption is studied.

The binding energy (E_{bind}) of all possible configurations of adsorption of Cu, CuO, or H_2S on GS is calculated by:

$$E_{bind} = E_{total} - (E_{GS} + E_{atomormolecule}) \quad (1)$$

where E_{total} is the total energy of the Cu, CuO or H_2S adsorbed GS, E_{GS} is the total energy of the GS, and $E_{atomormolecule}$ is the total energy of the free Cu atom, CuO, or H_2S molecule.

Moreover, to evaluate the binding energy between the H_2S and Cu-GS (H_2S/Cu-GS) or the H_2S and CuO-GS (H_2S/CuO-GS) structures, E_{bind} is used according to the following equation:

$$E_{bind} = E_{total} - \left(E_{structure} + E_{H_2S}\right) \quad (2)$$

where the E_{total} is the total energy of the Cu-GS or CuO-GS structures interacting with the H_2S gas. $E_{structure}$ is the total energy of the Cu-GS or CuO-GS structures, and E_{H_2S} is the total energy of the free H_2S gas. The most stable configuration happens when binding energy is more negative.

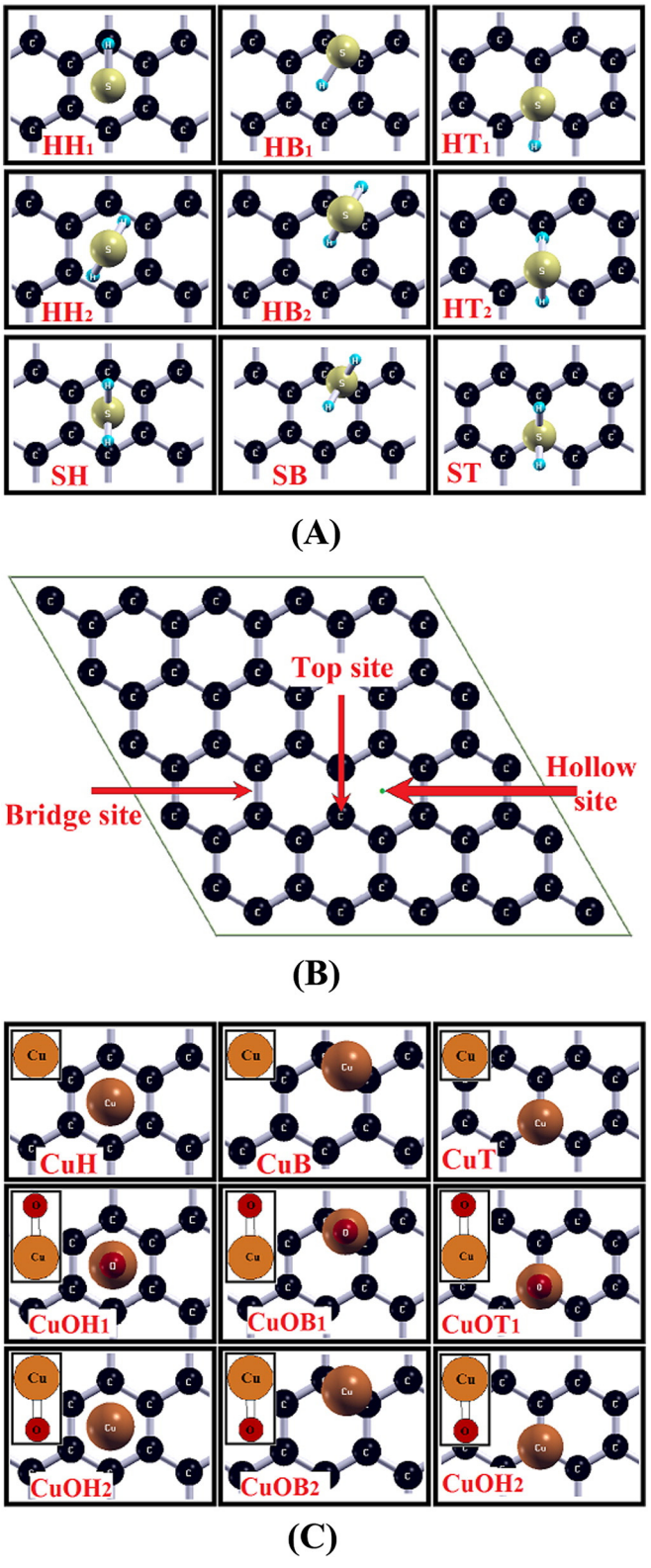

Fig. 1. (A) Schematic view of H_2S interacting with GS in 9 possible adsorption configurations (ST, SH, SB, HT_1, HH_1, HB_1, HT_2, HH_2, and HB_2), (B) schematic view of 3 positions for the adsorption of atom or molecule on GS, and (C) three different orientations for Cu nearing to GS (CuT, CuH, and CuB), and six different orientations for CuO nearing to GS ($CuOT_1$, $CuOH_1$, $CuOB_1$, $CuOT_2$, $CuOH_2$, and $CuOB_2$).

Table 1
Calculated adsorption energies (E_{bind}) and the binding length (d) of S–C or H–C in H_2S-GS using the PBE and vdW density functionals.

Method	PBE		vdW	
Sites	E_{bind} (eV)	d (Å)	E_{bind} (eV)	d (Å)
ST	−0.007	3.597	−0.125	2.890
SH	−0.018	4.025	−0.178	3.688
SB	−0.017	4.006	−0.174	3.560
HT_1	−0.020	2.648	−0.184	2.526
HH_1	−0.018	3.005	−0.157	2.907
HB_1	−0.018	2.742	−0.163	2.663
HT_2	−0.020	3.090	−0.183	3.054
HH_2	−0.022	3.149	−0.185	3.000
HB_2	−0.019	3.284	−0.085	3.190

3. Results and discussion

3.1. Adsorption of H_2S on the GS

To further understand the adsorption properties of H_2S gas adsorbed onto GS (H_2S-GS), we considered all possible adsorption configurations. An H_2S gas has two potential binding groups that can be close to the graphene layer (H and S atoms). Nine possible configurations — six configurations for the H atoms (HT_1, HH_1, HB_1, HT_2, HH_2, and HB_2) and three configurations for the S atom (ST, SH, and SB) — were investigated for the adsorption of H_2S onto GS, as they are shown in Fig. 1(A,B). As results for PBE in Table 1 show, the H_2S adsorption on the GS is a weak physisorption. So, only for this situation, the calculations are also done by using van der Waals density functional (vdW-DF) which has better consistency with experimental results for weak adsorptions [41–49]. The results based on vdW-DF calculations are shown in Table 1. According to the results of both PBE and vdW-DF, the HH_2 configuration is the most stable state after adsorption. The calculated adsorption energy value at the most stable position (HH_2) is −0.185 eV based on vdW-DF. Table 1 also demonstrates the adsorption distance (d) of the H_2S above the adsorbed GS, which is defined as the distance between center C atom of the GS and the closest atom of the H_2S to the GS. Considering all adsorption positions, the H_2S gas floated above the GS at a distance of around 2.526–3.688 Å.

DOS of H_2S-GS structure is calculated for HH_2 configuration by both PBE and vdW-DF and plotted in Fig. 2(A). Comparing the DOS of GS to that of H_2S-GS near the Fermi level, no considerable change and no evidence of hybridization between the H_2S gas and GS are observed.

To study the changes of electronic structure in GS caused by the adsorption of H_2S, the net charge transfer (Q_T) between the GS and the H_2S was calculated using Mulliken population analysis [50]. Electron charge transfer plays a significant role in the electronic properties and stability of an interacting system. The net charge transfer from GS to H_2S was computed to be 0.019 electrons by vdW and 0.0096 electrons by PBE which is consistent with the reported results [14]. Caution: there is no experimental test for the confirmation of results of such analyses.

To understand the enhancement effect of the attached C atom on the H2S adsorption, the PDOS of the S 3p, H 1s, and C 2p in H_2S-GS system based on both PBE and vdW is plotted in Fig. 2(B,C). The overlap between the S 3p orbital and C 2p orbital demonstrates that H_2S can weakly hybridize with GS. This result confirms that the adsorption of H_2S on the GS does not change its electronic properties and shows that only a weak interaction exists between the H_2S and the GS.

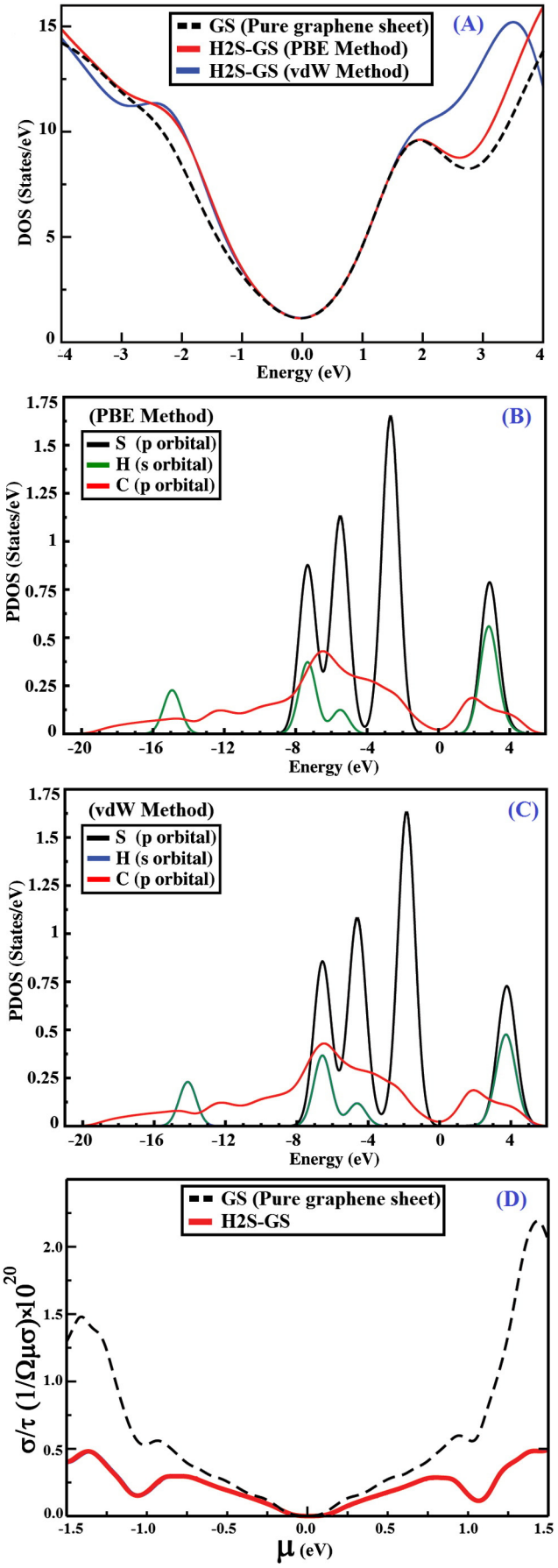

Fig. 2. (A) Calculated DOS for GS (black dots), and H_2S-GS structures for the HH_2 configuration by using both PBE (red line) and vdW (blue line), (B) the PDOS of C atoms of GS and the H and S atoms of H_2S-GS for (HH_2) configuration by using PBE, (C) the PDOS of C atoms of GS and the H and S atoms of H_2S-GS for (HH_2) configuration by using vdW, and (D) electrical conductance per relaxation time versus chemical potential at room temperature for GS (black dashes), and H_2S-GS (red line) with HH2 configuration. The Fermi level is set to zero. (For interpretation of the references to color in this figure legend, the reader is referred to the web version of this article.)

Next, the electrical conductance of H_2S-GS at room temperature is calculated and trace of conductance tensor is extracted by prefix.trace file which is an output of BoltzTrap code. Results show that conductance in x- and y-direction is identical. Also, in z-direction because of distance between graphene layers, conductance is very low which can be omitted. Variation of electrical conductance at room temperature versus chemical potential is plotted in Fig. 2(D). To plot Fig. 2(D), zero point of chemical potential is assumed to be the Fermi energy level. As this figure illustrates, in the Fermi level (E_F), electrical conductance of each mentioned configuration is similar to other ones. After H_2S adsorption on GS, conductance of structure, near the Fermi level decreases in comparison with conductance of GS. When H_2S is adsorbed on GS, the mobility of electrons is reduced which causes conductance reduction. Using the above calculations (binding energy, Q_T, PDOS, DOS, and electrical conductance), it is found that the interaction between H_2S and GS is a weak physisorption and GS is not a good adsorbent material for H_2S.

3.2. Adsorption of Cu, and CuO on the GS

In this step, the adsorption of Cu atom and CuO molecule onto a GS is investigated, Separately. The Cu-GS, and CuO-GS structures are modeled using one Cu atom, and CuO molecule per unit cell, adsorbed at different adsorption sites (Fig. 1(C)): the top site immediately above a C atom (CuT, CuOT1, and CuOT2), the hollow site at the center of a hexagon (CuH, CuOH1, and CuOH2), and the bridge site at the midpoint of a C–C bond (CuB, CuOB1, and CuOB2). According to the results for adsorption energies shown in Table 2, the CuB, and CuOB1 configurations are the most stable state after adsorption. As results show, the interaction between Cu and GS is physical and the interaction between CuO and GS is chemical. As it is demonstrated in Fig. 3(A,B), the distance between the Cu and the nearest carbon atom for Cu-GS is 2.22 Å, and the distance for CuO-GS is 2.16 Å.

We also plotted DOS curves to confirm the above findings about the type of adsorption. In Fig. 4(A), the DOS diagrams for the Cu-GS, and the CuO-GS systems are shown and compared to the DOS of the GS. Also, for the two systems, PDOS of the 3d, and 4s for Cu and 2p for C atoms are plotted in Fig. 4(B). Using PDOS results, the net charge transfer for both structures is obtained: for Cu-GS, 0.354 electrons are transferred from the Cu to the GS; and for CuO-GS, 0.074 electrons are transferred from the CuO to the GS. The overlap between the 3d and 4s orbitals of Cu and 2p orbital of C indicates that hybridization in CuO-GS is stronger than the Cu-GS system.

Next, the electrical conductance of both structures at room temperature is calculated. Variation of electrical conductance versus chemical potential is plotted in Fig. 4(C). As this figure illustrates, in the Fermi level (E_F), electrical conductance of each forenamed system is different from the other one. After Cu adsorption on GS, conductance of structure, near the Fermi level increases in comparison with conductance of GS. When Cu is adsorbed on GS, the mobility of electrons is increased which leads to higher conductance. Near the Fermi level, the electrical conductance at room temperature for CuO-GS compared with GS is relatively constant.

Using the binding energy, DOS, PDOS, and electrical conductance calculations, we find that the interaction between Cu and GS is a weak physisorption, and the interaction between CuO and GS is chemisorption.

3.3. H_2S adsorption on Cu-GS, and CuO-GS

We performed DFT calculations to investigate the most stable adsorption geometry of H_2S gas, with either the H or S atom nearest to the Cu-GS and the CuO-GS. It is found that H_2S prefers to adhere to the Cu-GS surface with the S atom, and adhere to the CuO-GS surface with the H atom. Fig. 5(A,B) demonstrates the optimized structures with binding lengths for H_2S/Cu-GS, and H_2S/CuO-GS configurations.

Table 2
Calculated values of adsorption energies (E_{bind}) and the binding length (d) of Cu–C in Cu-GS, and CuO-GS.

Sites	E_{bind} (eV)	d (Å)
CuT	−0.239	2.118
CuH	−0.031	3.320
CuB	−0.242	2.218
$CuOT_1$	−0.840	2.083
$CuOH_1$	−0.640	2.460
$CuOB_1$	−0.870	2.160
$CuOT_2$	−0.240	3.273
$CuOH_2$	−0.256	3.119
$CuOB_2$	−0.260	3.000

According to the calculations, the magnitude of the adsorption energies for the H_2S/Cu-GS, and H_2S/CuO-GS configurations are relatively large, equal to −0.88 eV, and −1.23 eV, respectively. This adsorption energies obtained for H_2S/Cu-GS, and H_2S/CuO-GS are larger than that of the modeled H_2S-GS system, indicating that the presence of Cu, or CuO increases the capability of GS to adsorb H_2S. According to these results, the interaction between H_2S and both structures is chemical. Due to stronger interaction, the CuO-GS is better than the Cu-GS for H_2S adsorption.

The adsorption mechanisms are discussed in terms of the Mulliken population analysis, and DOS and PDOS plots, which can provide clear, definitive descriptions of charge redistribution. DOS of GS, Cu-GS, and CuO-GS structures before and after H_2S adsorption is plotted in Fig. 6(A). As it is observable from adsorption energies and Fig. 6(A), DOS of each mentioned configuration is different from the other ones. Also, the Q_T results are supported by the data from Mulliken charge analysis and show that for Cu-GS surface, 0.132 electrons are transferred from the H_2S to the Cu. Also, results show that after H_2S adsorption, 0.842 electrons are transferred from Cu to GS. To understand the enhancement effect of the attached Cu atom on the H2S adsorption, the PDOS of the S 3p and Cu 3d in H_2S/Cu-GS complex were plotted, as shown in Fig. 6(B). The overlap between the S 3p orbital and Cu 3d, and 4s orbitals demonstrates that H_2S can weakly hybridize with Cu-GS. According to the calculation result, after the adsorption of H_2S on CuO-GS surface, 0.084 electrons are transferred from the H_2S to the CuO. Also, when the CuO decorated on the GS encounters H_2S, the transferred electrons from H_2S to CuO are easily extracted by GS. the PDOS of the S 3p, Cu 3d, and O 2p orbitals in H_2S/CuO-GS is plotted in Fig. 6(B). The overlap between the S 3p, O 2p, and Cu 3d orbitals demonstrates that H_2S can strongly hybridize with CuO. In addition, our calculation reveals that the two systems after H_2S adsorption, the transferred electrons from H_2S to Cu, and CuO are easily extracted by GS. Therefore, using the binding energy, Q_T, and PDOS, it is found that, in the same

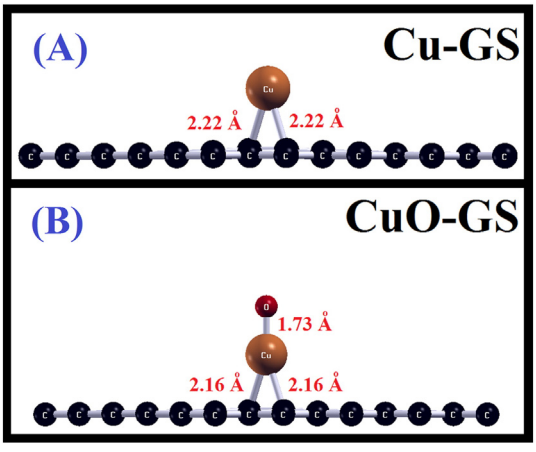

Fig. 3. (A) Optimized configuration of Cu-GS (CuB). (B) Optimized configuration of CuO-GS ($CuOB_1$).

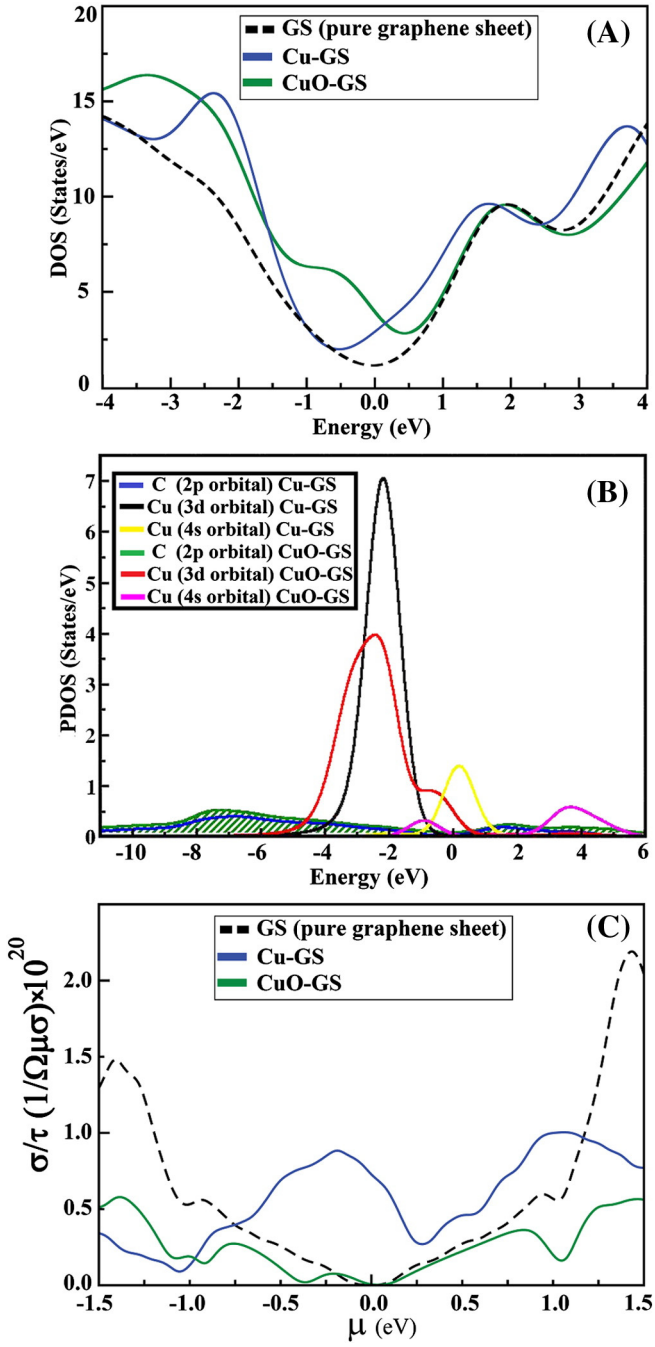

Fig. 4. (A) Calculated DOS for GS (black dashes), Cu-GS with CuB configuration (blue line),and CuO-GS with CuOB1 configuration (green line), (B) the PDOS of C and Cu atoms in Cu-GS (CuB configuration) and CuO-GS (CuOB1 configuration), and (C) electrical conductance per relaxation time versus chemical potential at room temperature for Cu-GS with CuB configuration (blue line),and CuO-GS with CuOB1 configuration (green line). The Fermi level is set to zero. (For interpretation of the references to color in this figure legend, the reader is referred to the web version of this article.)

conditions, the CuO-GS has more favorable features in the adsorption of H_2S than the Cu-GS.

To understand more of the electronic properties of H_2S/Cu-GS, and H_2S/CuO-GS, the electrical conductance at room temperature is calculated for both structures and is plotted versus chemical potential in Fig. 7. As this figure illustrates, in the Fermi level, electrical conductance of each mentioned configuration is different from other ones. After H_2S adsorption on the Cu-GS, conductance of structure, near the Fermi level, decreases in comparison with conductance of the Cu-GS. But after the adsorption of H_2S on CuO-GS, conductance of structure, near the

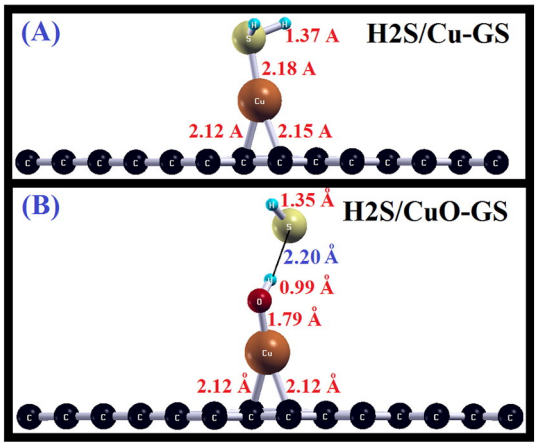

Fig. 5. (A) Optimized configuration of H_2S/Cu-GS. (B) Optimized configuration of H_2S/CuO-GS.

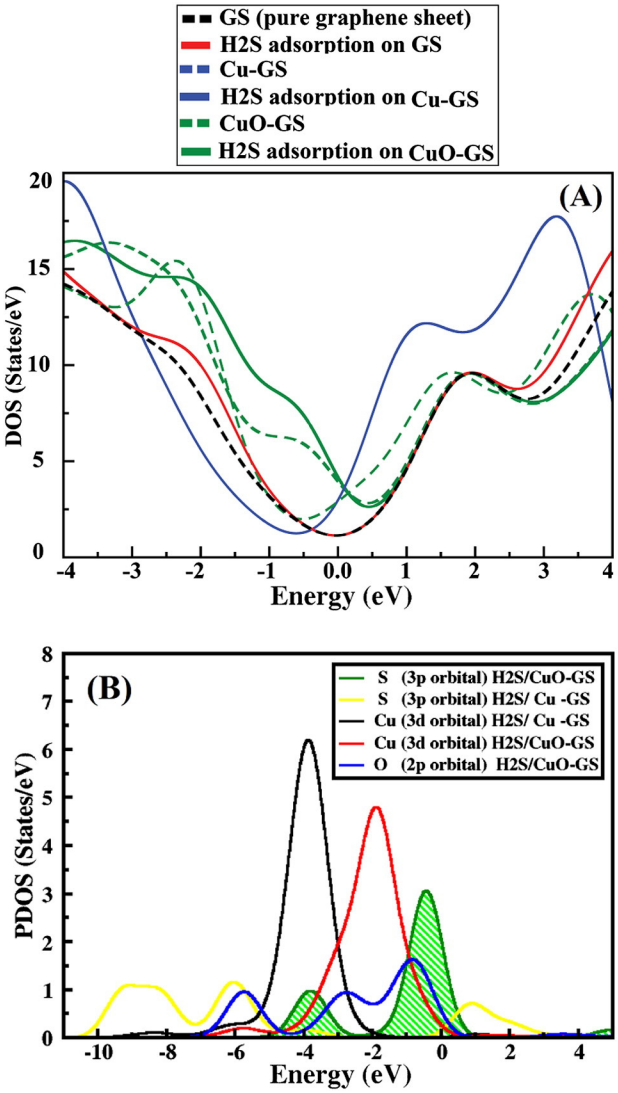

Fig. 6. (A) Calculated DOS for H_2S/Cu-GS (blue line),and H_2S/CuO-GS (green line) for the most stable configuration and GS (black dashes), CuB configuration of Cu-GS (blue dashes) and CuOB1 configuration of CuO-GS (green dashes). (B) The PDOS of S and Cu atoms of optimized H_2S/Cu-GS and the PDOS of S, Cu and O atoms of optimized H_2S/CuO-GS configurations. The Fermi level is set to zero. (For interpretation of the references to color in this figure legend, the reader is referred to the web version of this article.)

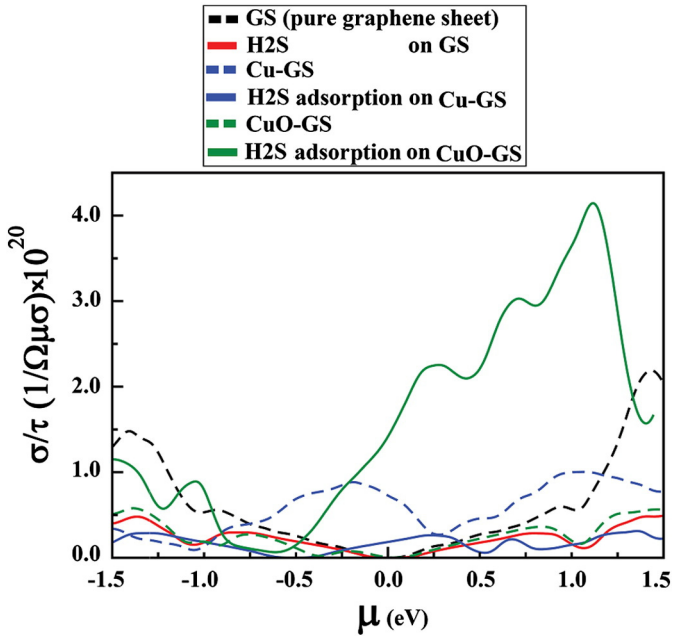

Fig. 7. Electrical conductance per relaxation time versus chemical potential at room temperature for GS (black dashes), HH_2 configuration of H_2S-GS (red line), CuB configuration of Cu-GS (blue dashes), H_2S/Cu-GS (blue line), $CuOB_1$ configuration of CuO-GS (green dashes), and H_2S/CuO-GS (green line) structures. The Fermi level is set to zero. (For interpretation of the references to color in this figure legend, the reader is referred to the web version of this article.)

Fermi level increases in comparison with conductance of CuO-GS surface. Also, near the Fermi level, the electrical conductance at room temperature for H_2S/CuO-GS compared with H_2S/Cu-GS and H_2S-GS is significantly high. This fact demonstrates that the CuO-GS is the best nanosensor for H_2S detection in comparison with Cu-GS and GS.

4. Conclusion

In this paper, adsorption mechanisms of H_2S onto GS, Cu-GS and CuO-GS in addition to the electrical conductance of GS, H_2S-GS, Cu-GS, CuO-GS, H_2S/Cu-GS and H_2S/CuO-GS are investigated and calculated using DFT method to study H_2S detection. The adsorption of H_2S onto GS was very weak due to its small adsorption energy, and small net charge transfer between the GS and H_2S. After H_2S adsorption on GS, conductance of structure at room temperature, in the Fermi level is similar, and near the Fermi level decreases in comparison with conductance of GS. To elevate the adsorption effect, a Cu atom, and CuO molecule were attached to the GS, separately. Strong adsorption was found due to a large adsorption energy compared to those of the H_2S-GS configuration. Furthermore, the DOS was calculated and the results showed that there was no impressive evidence for hybridization between the H_2S and the GS, while a weak interaction between H_2S and the Cu-GS happened. Contrary to two mentioned structures, CuO-GS has a strong interaction with H_2S. Next, electrical conductance is computationally investigated. Interestingly, the obtained results illustrate that electrical conductance of the CuO-GS, and Cu-GS is significantly changed by H_2S gas adsorption. Also, results demonstrate in the same conditions and at room temperature, that the CuO-GS system has more favorable features in the detection of H_2S than the Cu-GS. The results presented in this paper provide helpful information for the detection of H_2S by CuO-GS nanosensor.

Appendix A. Supplementary data

Supplementary data to this article can be found online at http://dx.doi.org/10.1016/j.susc.2015.02.002.

References

[1] P. Cosoli, M. Ferrone, S. Pricl, M. Fermeglia, Chem. Eng. J. 145 (2008) 86.
[2] M. Cakmak, G.P. Srivastava, Phys. Rev. B 57 (1998) 4486.
[3] M. Cakmak, G.P. Srivastava, Phys. Rev. B 60 (1999) 5497.
[4] J. Guo, Y. Luo, A.Ch. Lua, R.-A. Chi, Y.-L. Chen, X.-T. Bao, Sh.-X. Xiang, Carbon 45 (2007) 330.
[5] M. Asada, M.H. Sheikhia, Sensors Actuators B 198 (2014) 134.
[6] S. Nishimura, M. Yoda, Water Sci. Technol. 36 (1997) 349.
[7] S. Mubeen, T. Zhang, N. Chartuprayoon, Y. Rheem, A. Mulchandani, N.V. Myung, M.A. Deshusses, Anal. Chem. 82 (2010) 250.
[8] S. Steinhauer, E. Brunet, T. Maier, G.C. Mutinati, A. Kock, Sensors Actuators B 186 (2013) 550.
[9] A. Chowdhuri, P. Sharma, V. Gupta, K. Sreenivas, K.V. Rao, J. Appl. Phys. 92 (2002) 2172.
[10] Y.-C. Chung, Y.-Y. Lin, C.-P. Tseng, Bioresour. Technol. 96 (2005) 1812.
[11] X. Jiang, J.H. Tay, J. Hazard. Mater. 176 (2010) 638.
[12] L.M. Leuch, A. Subrenat, P.L. Cloirec, Langmuir 19 (2003) 10869.
[13] S. Bashkova, F.S. Baker, X. Wu, T.R. Armstrong, V. Schwartz, Carbon 45 (2007) 1354.
[14] M.D. Ganji, N. Sharifi, M. Ardjmand, M. Ghorbanzadeh Ahangari, Appl. Surf. Sci. 261 (2012) 697.
[15] S. Sharma, A.S. Verma, Physica B 427 (2013) 12.
[16] Y.y. Shao, J. Wang, H. Wu, J. Liu, I.A. Aksay, Y. Lin, J. Electroanalysis 22 (2010) 1027.
[17] H.H. Pu, S.H. Rhim, M. Gajdardziksa-Josifovska, C.J. Hirschmugl, M. Weinert, J.H. Chen, RSC Adv. 4 (2014) 47481.
[18] D. Ye, G. Liang, H. Li, J. Luo, S. Zhang, H. Chen, J. Kong, Talanta 116 (2013) 223.
[19] B. Wang, X.L. Wu, C. Shu, Y.G. Guo, C.R. Wang, J. Mater. Chem. 20 (2010) 10661.
[20] K. Jagannadham, Metall. Mater. Trans. B 43B (2012) 316.
[21] L. Zhou, F. Shen, X. Tian, D. Wang, T. Zhang, W. Chen, Nanoscale 5 (2013) 1564.
[22] I.V. Lightcap, T.H. Kosel, P.V. Kamat, Nano Lett. 10 (2010) 577.
[23] S. Cui, H. Pu, E.C. Mattson, G. Lu, S. Mao, M. Weinert, C.J. Hirschmugl, M. Gajdardziska-Josifovskab, J. Chen, Nanoscale 4 (2012) 5887.
[24] S. Cui, H. Pu, G. Lu, Z. Wen, E.C. Mattson, C. Hirschmugl, M. Gajdardziska-Josifovska, M. Weinert, J. Chen, ACS Appl. Mater. Interfaces 4 (2012) 4898.
[25] T.T. Baby, R. Sundara, J. Phys. Chem. C 115 (2011) 8527.
[26] H. Yu, J. Yu, S. Liu, S. Mann, Chem. Mater. 19 (2007) 4327.
[27] R.P. Wijesundera, Semicond. Sci. Technol. 25 (2010) 045015.
[28] S. Anandan, X. Wen, S. Yang, Mater. Chem. Phys. 93 (2005) 35.
[29] L.C. Jiang, W.D. Zhang, Biosens. Bioelectron. 25 (2010) 1402.
[30] T. Fu, Electrochim. Acta 112 (2013) 230.
[31] A. Comanac, L. De Medici, M. Capone, A.J. Millis, Nat. Phys. 4 (2008) 287.
[32] S. Gao, S. Yang, J. Shu, S. Zhang, Z. Li, K. Jiang, J. Phys. Chem. C 112 (2008) 19324.
[33] Y.J. Mai, X.L. Wang, J.Y. Xiang, Y.Q. Qiao, D. Zhang, C.D. Gu, J.P. Tu, Electrochim. Acta 56 (2011) 2306.
[34] S. Liu, J. Tian, L. Wang, Y. Luoa, X. Sun, Catal. Sci. Technol. 2 (2012) 339.
[35] D. Qiu, B. Zhao, Z. Lin, L. Pu, L. Pan, Y. Shi, Mater. Lett. 105 (2013) 242.
[36] X. Zhou, J. Zhang, Q. Su, J. Shi, Y. Liu, G. Du, Electrochim. Acta 125 (2014) 615.
[37] N. Yusoff, N.M. Huang, M.R. Muhamad, S.V. Kumar, H.N. Lim, I. Harrison, Mater. Lett. 93 (2013) 393.
[38] E. Mohammadi-Manesh, M. Vaezzadeh, M. Saeidi, Comput. Mater. Sci. 97 (2015) 181.
[39] P. Giannozzi, S. Baroni, N. Bonini, M. Calandra, R. Car, C. Cavazzoni, et al., Condens. Matter 21 (2009) 395502.
[40] G.K.H. Madsen, D.J. Singh, Comput. Phys. Commun. 175 (2006) 67.
[41] M.A. Neumann, M.A. Perrin, J. Phys. Chem. B 109 (2005) 15531.
[42] E. Hult, Y. Andersson, B.I. Lundqvist, D.C. Langreth, Phys. Rev. Lett. 77 (1996) 2029.
[43] E. Hult, H. Rydberg, B.I. Lundqvist, D.C. Langreth, Phys. Rev. B 59 (1999) 4708.
[44] M. Dion, H. Rydberg, K.E. Schoroder, B.I. Langreth, B.I. Lundqvist, Phys. Rev. Lett. 92 (2004) 246401.
[45] J.F. Dobson, J. Wang, Phys. Rev. B 62 (2000) 038.
[46] W. Kohn, Y. Meir, D.E. Makarov, Phys. Rev. Lett. 80 (1998) 4153.
[47] A.J. Du, Sean C. Smith, Nanotechnology 16 (2005) 2118.
[48] V.I. Hegde, S.N. Shirodkar, N. Tit, U.V. Waghmare, Z.H. Yamani, Surf. Sci. 621 (2014) 168.
[49] S. González, F. Viñes, J.F. García, Y. Erazo, F. Illas, Surf. Sci. 625 (2014) 64.
[50] R.S. Mulliken, J. Chem. Phys. 23 (1955) 1833.